Available online at www.sciencedirect.com
ScienceDirect
International Journal of Heat and Fluid Flow 28 (2007) 932–937
International Journal of HEAT AND FLUID FLOW
www.elsevier.com/locate/ijhff

Aerodynamics and heat transfer predictions in a highly loaded turbine blade

Yi Liu *

Department of Engineering Science, University of Oxford, Oxford OX1 3PJ, United Kingdom

Received 6 December 2005; received in revised form 22 February 2007; accepted 23 February 2007
Available online 15 May 2007

Abstract

We numerically investigate the transonic viscous flow and heat transfer in a highly loaded turbine blade, where the interaction of a shock wave, a wake and a boundary layer often leads to very complicated flow phenomena. The numerical method, a modified implicit flux-vector-splitting (MIFVS) solver of the Navier–Stokes equations, which has been well established by combining a unique implicit formulation with a flux-vector-splitting scheme, is extended to simulate such transonic cascade flow. Turbulence is modeled with a low Reynolds number k–ϵ model which also considers the compressibility effects. The laminar to turbulent transition is well captured by implementing transitional parameters into the damping function of k–ϵ model. With this extended MIFVS solver, we efficiently predict the heat transfer, shock and boundary layer interactions in the VKI highly loaded transonic turbine blade. The obtained results show good agreement with the experimental data and other published calculation results. The main flow features are well predicted.

Keywords: Boundary layer; Heat transfer; Highly loaded; Shock; Turbine blade; Turbulence

1. Introduction

Through continuous and rapid development in computational fluid dynamics (CFD), significant advances have been made to turbine blades both in their loading and design philosophy (Curtis et al., 1996). In recent years, efforts have been directed to design blades with increasing aerodynamic loading (lift coefficient), leading to the so-called high lift profiles. The large pressure ratio and high loading coefficient in such turbine blades could cause a complicated transonic flow pattern with shock waves and separated zones, especially in blades with a large blade turning angle and a high exit Mach number. To design and optimize these turbines, it is imperative for these interactions to be thoroughly understood. A key numerical challenge in meeting this goal is to accurately model the main flow field while maintaining a high numerical efficiency.

The performance of highly loaded turbine blades has been actively studied both by experiment and numerically (Chima, 1996; Curtis et al., 1996; Howell et al., 2000; Gehrer and Jericha, 1998; Granovskii et al., 1995; Howell et al., 2001; Hall et al., 1998; Sarkar, 2005; Segawa et al., 2001). The work, for example, has been directed at reducing both the weight and the manufacturing cost of modern aircraft engines (Howell et al., 2000; Segawa et al., 2001).

For design and analysis of these turbine blades, reliable computational methods are essential, with realistic simulation of turbulence and transition processes (Michelassi and Rodi, 1997). The important parameters of interest include the accurate prediction of heat transfer, wake mixing, and the interactions among a shock wave, a boundary layer and a wake.

A modified implicit flux-vector-splitting (MIFVS) numerical solver has been previously developed and applied to various other flow analyses (Liu et al., 1996; Liu and Kendall, 2004; Liu and Bellhouse, 2005; Liu and Zhang, 2006). Numerical simulations have shown that

* Tel.: +44 1865 274740.
E-mail address: yi.liu@eng.ox.ac.uk

0142-727X/$ - see front matter © 2007 Elsevier Inc. All rights reserved.
doi:10.1016/j.ijheatfluidflow.2007.02.009

Nomenclature

c, c_{ax}	chord, axial chord (m)
c_p	specific heat at the constant pressure (J/kg K)
e	total energy (J/kg)
J	Jacobi
k	turbulence kinetic energy (J/kg)
Ma	Mach number
p	static pressure (Pa)
P_k	production of turbulence kinetic energy (W/m^3)
$\dot{q}_i$	component of the heat flux vector (W/m^2)
Re	Reynolds number
s	surface length (m)
u_i	component of the cartesian velocity vector (m/s)
t	time (s)
T	temperature (K)
τ_{ij}	component of the shear stress tensor (N/m^2)
ϵ	dissipation of turbulence kinetic energy (J/kg s)
δ_{ij}	Kronecker's delta function
μ	viscosity (Ns/m^2)
ρ	density (kg/m^3)
ξ_i	general coordinates
$C_{\epsilon 1}$, $C_{\epsilon 2}$, C_μ, σ_k, σ_ϵ	turbulence model constants
f_1, f_2, f_μ	damping functions of k–ϵ model

Subscript

l, t	laminar, turbulent contribution
1, 2	inlet, outlet

Superscript

lam, turb	laminar, turbulent part
$'$	fluctuation

the MIFVS has significant advantages in terms of accuracy, convergence and computing cost.

The objective of this paper is to extend the MIFVS solver to the transonic cascade flow in a highly loaded turbine blade. New challenges here require accurate turbulence and transition models into the MIFVS code. Furthermore, the leading edge correction for turbulent production term needs to be included to improve calculation procedure. The approaches and methodologies to achieve these code improvements are presented and discussed. The performance of the MIFVS method is assessed by extensive comparisons with the experiment and available computed results for the transonic VKI highly loaded vane (Arts et al., 1990, 1994).

2. Governing equations

The equations used to model the cascade flow through stator and/or rotor blades are the compressible, Reynolds-averaged continuity, momentum and energy equations written in terms of generalized coordinates and in a conservative flux-vector-splitting form

$$\frac{\partial \widehat{U}}{\partial t}+\frac{\partial \widehat{F}_i^+}{\partial \xi_i}+\frac{\partial \widehat{F}_i^-}{\partial \xi_i}+\widehat{S}_1=\frac{1}{Re}\left[\frac{\partial \widehat{F_{vi}}}{\partial \xi_i}+\widehat{S}_2\right]. \tag{1}$$

More details can be found in Liu et al. (1996) and Liu and Bellhouse (2005).

3. Models for turbulence and transition

3.1. Turbulent stresses

The turbulence model used in this study is based on the Boussinesq's approximation that the principal axes of the turbulent stress tensor are coincident with those of the mean strain-rate tensor. This assumption makes it possible to close the Reynolds-averaged Navier–Stokes (RANS) equations by expressing the turbulent stresses, τ_{ij}^{turb}, with an eddy viscosity, μ_t, as

$$\tau_{ij}^{\text{turb}}=\overline{\rho u_i' u_j'}=\mu_t\left(\frac{\partial u_i}{\partial x_j}+\frac{\partial u_j}{\partial x_i}-\frac{2}{3}\frac{\partial u_k}{\partial x_k}\delta_{ij}-\frac{2}{3}\rho k\delta_{ij}\right). \tag{2}$$

Therefore, the RANS equations can be treated in a similar manner as the Navier–Stokes (NS) equations in the laminar flow, in which the molecular (laminar) viscosity, μ_l, is substituted by the effective viscosity, $\mu_l+\mu_t$.

3.2. Low Reynolds number k–ϵ turbulence model

Various low-Reynolds number k–ϵ turbulence models have been developed with different damping functions, constants and variation in source terms. Also boundary conditions may vary between some models. In general, all the low Reynolds number k–ϵ models can be rewritten in a form similar to Eq. (1)

$$\frac{\partial \widehat{U}^{k\epsilon}}{\partial \tau}+\frac{\partial (\widehat{F}_i^+)^{k\epsilon}}{\partial \xi_i}+\frac{\partial (\widehat{F}_i^-)^{k\epsilon}}{\partial \xi_i}+\widehat{S}_1^{k\epsilon}=\frac{1}{Re}\left[\frac{\partial \widehat{F_{vi}}^{k\epsilon}}{\partial \xi_i}+\widehat{S}_2^{k\epsilon}\right]. \tag{3}$$

Eq. (3) adopted here mainly indicate the relationship between the two-equation k–ϵ turbulence model and the RANS equations. These similarities make it straightforward to extend the method of implicit formulation and eigenvalue analysis of the NS to the turbulence model equations.

The nonlinear eddy-viscosity models (e.g., Craft et al., 1997) are regarded to have a better capability of predicting "by-pass" or "diffusion-controlled" transition phenomenon. However, there are many empirical coefficients and constants need to be elaborately calibrated before it can

be confidently applied for routine engineering applications. To demonstrate the methodology of the extended MIFVS solver, in this study, a linear eddy-viscosity k–ϵ model is rather adopted due to its robustness and a large spectrum of applicabilities.

The low Reynolds number model proposed by Chien (1982), together with Sarkar's compressibility modification (Sarkar et al., 1991), is implemented into the MIFVS code to simulate the turbulent boundary layer and the interaction with the shock wave. The damping functions and model constants of Eq. (3) are defined

$$\begin{aligned} &f_\mu = 1-\exp(-0.0115y^+);\\ &f_1 = 1.0;\\ &f_2 = 1-0.22\exp[-(Re_t/6)^2];\\ &Re_t = \frac{\rho k^2}{\mu\bar{\epsilon}};\quad y^+ = \frac{y\rho U^*}{\mu};\\ &C_\mu = 0.09;\quad C_{\epsilon 1} = 1.35;\quad C_{\epsilon 2} = 1.80;\quad \sigma_k = 1.0;\quad \sigma_\epsilon = 1.3. \end{aligned} \tag{4}$$

Most k–ϵ turbulence models are found to predict excessive levels of turbulent energy in stagnation regions, as often shown in the blunt leading edge of the highly loaded transonic turbine blades (Michelassi and Rodi, 1997). In this study, an approach for the leading edge correction proposed by Kato and Launder (1993) is adopted to reformulate the turbulent energy production term (P_k).

3.3. Transition model

In the transonic highly loaded turbine blade flow, the transition is normally of the by-pass type, which may be induced by an incoming free-stream turbulence, or triggered by a local flow separation or a shock. The nature transition is unlikely to take place in cascade flows (e.g. of the configuration in Fig. 1). The model embodied in the low Reynolds number k–ϵ turbulent model is described as follows.

The damping function of Eq. (4), f_μ, is modified to include a ratio of $25/A^+$ (Cho et al., 1993), which represents an intermittency function

$$f_\mu = 1-\exp\left(-0.0115y^+\frac{25}{A^+}\right). \tag{5}$$

The parameter A^+ is set to a critical value (e.g., 300) in laminar flows to guarantee the turbulence viscosity, μ_t, very small. The normal expression of f_μ (Eq. 4) is restored for fully turbulent boundary layer when A_t^+ equals 25. In the transitional region, A^+ is calculated by

$$A^+ = A_t^+ + (300 - A_t^+)\times\left[1-\sin\left(\frac{\pi}{2}\frac{Re_\theta - Re_{tr}}{Re_{tr}}\right)\right]^2$$

in which Re_{tr} is specified by the following empirical relation (Abu-Ghannam and Shaw, 1980)

$$Re_{tr} = 163 + \exp\left(F(\lambda) - \frac{F(\lambda)\mathrm{Tu}}{6.91}\right).$$

The transition model is implemented only inside the boundary layer. The flow is turbulent outside the boundary layer in the full developed turbulent cascade flow. The damping functions of Eqs. (4) and (5) are evaluated accordingly.

4. Numerical implementation

4.1. Implicit scheme

The implicit formulation of Eq. (1), also applicable to Eq. (3) of the low Reynolds number k–ϵ model, is described in the semi-discrete delta form

$$\begin{aligned} \frac{\partial(\delta\widehat{U}^{n+1})}{\partial t} = \frac{\Delta\widehat{U}^n}{\Delta t} + \Bigg[&-\sum_{i=1}^{3}\frac{\partial(\lambda_i^+\delta\widehat{U}^{n+1}+\lambda_i^-\delta\widehat{U}^{n+1})}{\partial\xi_i} - \lambda_{1s}\delta U^{n+1}\\ &+\sum_{i=1}^{3}\frac{\partial(\lambda_{vi}\delta\widehat{U}^{n+1})}{\partial\xi_i}+\sum_{i=1}^{3}\frac{\partial(\lambda_{2s}\delta\widehat{U}^{n+1})}{\partial\xi_i}\Bigg];\\ \widehat{U}^{n+1} = \widehat{U}^n + \delta\widehat{U}^{n+1} \end{aligned} \tag{6}$$

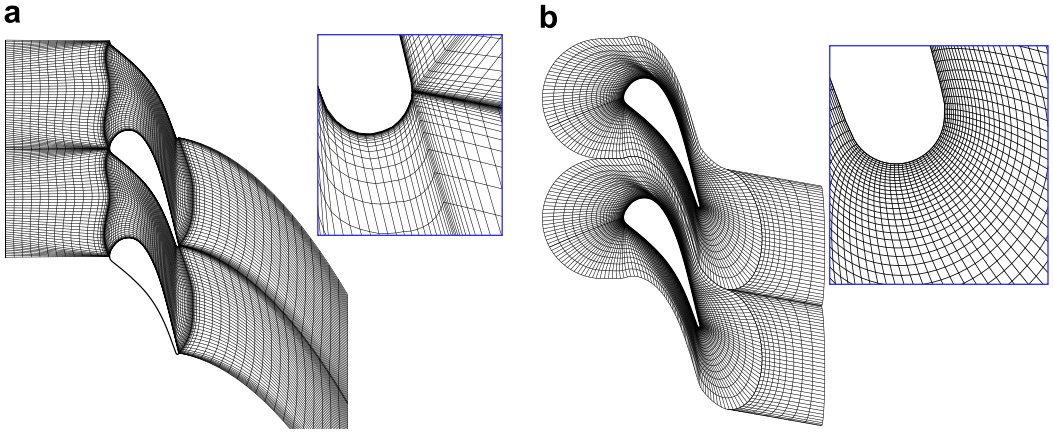

Fig. 1. Computational domain and grids, with the trailing edge magnified: (a) periodic H-mesh and (b) periodic O-mesh patched with H-mesh.

where $\lambda_i^{\pm}$, λ_{vi}, λ_{1s} and λ_{2s} are the spectral radii of Jacobian matrices of the convection, dissipation and source terms respectively. $\Delta\widehat{U}^n$ is evaluated in explicit step by a second-order accuracy flux-vector-splitting (FVS) scheme (Steger and Warming, 1981). Meanwhile, first-order time- and spatial-difference schemes are used for the implicit part due to steady problems. The resultant implicit algebraic equations can be solved efficiently. The convergence rate is further accelerated by a multi-grid technique.

4.2. Multi-block structure and computational grid

In this study, a multi-block topology is employed to generate a better quality grid for the highly loaded turbine blade with a large turning angle and a blunt leading/trailing edge. Various grid densities and nodal distributions have been used to study the influence of the discretization on the physical domain. All the results presented have been verified on different grids (from 9000 to 40000 cells) to ensure grid-independent solutions.

Fig. 1 shows typical periodic cascade grids (every other point), in which the blade is embodied in the computational domain. The grid shown in Fig. 1a is a fully H-mesh. The periodic boundary is preserved by the nodal periodic distributions. The grid in Fig. 1b is a basically periodic O-mesh, in which the orthogonal meshing is implemented around the blade, patched with an outlet periodic H-mesh. Numerical simulations show such periodic O-mesh obtained slightly better results near the trailing edge when the vortex shedding exists. For heat transfer calculations, the first grid point adjacent to the blade surface is placed at $y^+ \approx 0.2$–0.8, with approximately 30 points within the boundary layer.

5. Results and discussion

5.1. Validation: a high-loaded transonic VKI vane

A highly loaded transonic turbine nozzle guide vane (NGV) has been selected and calculated in this paper due to a wealth of experimental data available (Arts et al., 1990; Arts, 1994). The NGV was performed in the Isentropic Light Piston Compression Tube facility in the von Karman Institute (VKI). This facility has independent control over the exit Mach number ($Ma_{2,is}$), the exit Reynolds number (Re_2), inlet turbulence intensity (Tu), and the gas to the wall temperature ratio.

As a validation, we firstly simulate the case with low and medium exit Mach numbers (0.84 and 1.02, respectively), with an aim at assessing the accuracy and robustness of the extended MIFVS method. Computed wake profiles located at 43.3% of axial chord downstream of the trailing edge are compared to the experimental data, digitized manually from (Arts et al., 1990), in Fig. 2. A better agreement in the lower Mach number case is seen. In contrast, a rather large discrepancy is found for the exit Mach number of 1.02 case. This is probably due to the lack of fidelity of linear turbulence model in the complex flow region (e.g., separation), and the fact that both simulations were performed on the same grid. It should be pointed out that the measured and computed integrals are almost identical, when considering the difference of flow condition.

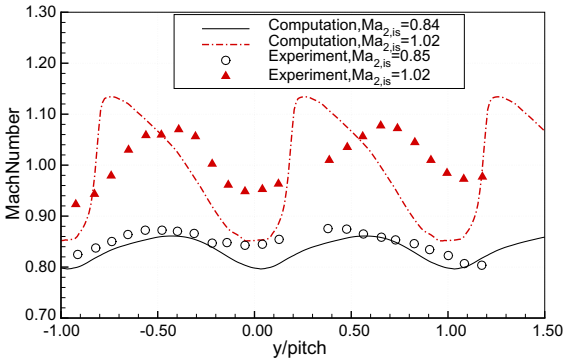

Fig. 2. Wake profiles of Mach number.

Further interrogations of the surface Isentropic Mach number distributions (Fig. 3) and density gradient contours (numerical Schlieren, not shown) obtain a better agreement with experimental measurements.

5.2. VKI MUR235 test case: lower exit Mach number

The flow conditions of the VKI MUR235 test case correspond to an exit isentropic Mach number of $Ma_{2,is} = 0.927$, an exit Reynolds number of $Re_2 = 1.25 \times 10^6$ and a free stream turbulence intensity of Tu = 6%.

The contour plots of Mach number in Fig. 4 are obtained with the low Reynolds number k–ϵ turbulence model and Kato and Launder correction. Clearly it shows that the problem with the high levels of kinetic energy in the stagnation region, as illustrated in Fig. 4.3 by Gehrer and Jericha (1998), has been improved.

Fig. 5 illustrates the respective heat flux distributions for the MUR235 case. The effects of turbulence length scale have been examined for the same flow condition. The transition is predicted slightly too early on the suction side for a

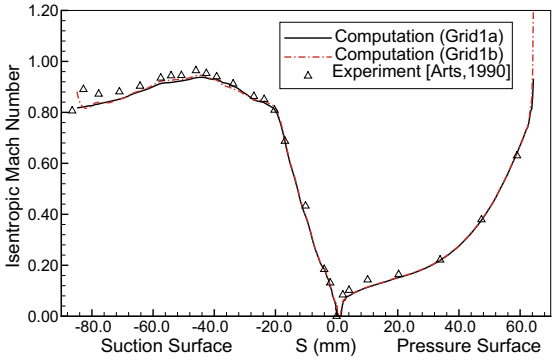

Fig. 3. Isentropic Mach number distributions.

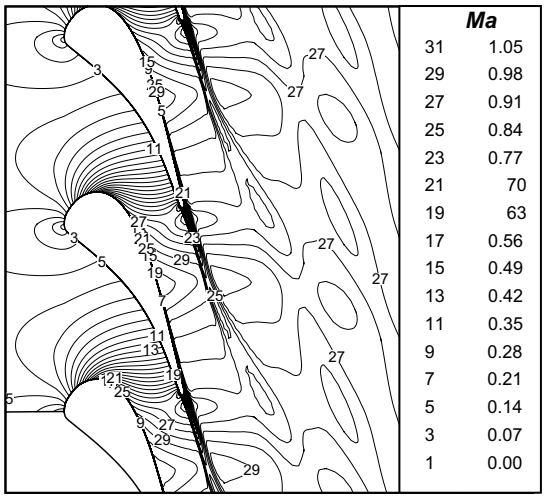

Fig. 4. Contour plots of Mach number for the VKI MUR235.

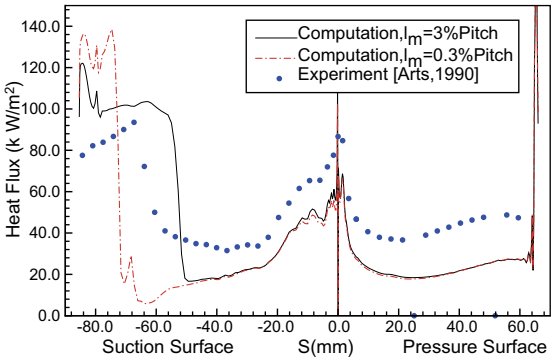

Fig. 5. Heat flux distributions for the VKI MUR235.

turbulence length scale (l_m) of 3% pitch. Decreasing l_m by a factor of 10 to a value of $l_m = 0.3\%$ pitch causes the transition move downstream. On the pressure side, the predicted heat flux levels are lower than experimental data for both length scales, which are consistent with other published numerical results in the same VKI MUR235 studies (Hall et al., 1998; Gehrer and Jericha, 1998; Chima, 1996).

Often, the ϵ value, corresponding to turbulence length scale l_m, is ambiguous at the inflow boundary. To the authors' best knowledge, the selected value of l_m varies significantly in the literature even for the same VKI case study. For example, the turbulence length scale l_m was set to 10% of pitch by Hall et al. (1998). Gehrer and Jericha (1998), in their study, gave a comparison of the calculated results with l_m of 0.425% and 4.25% of pitch. Chima, meanwhile, covered a even wider range from 0.015% to 1.74% of pitch and concluded the best prediction for transition is about 0.06% (Chima, 1996). All the studies indicate that the transition is evidently influenced by the turbulence length scale.

Nevertheless, as shown in Fig. 5, the model captures the overall behavior quite well, although the predicted heat flux level is a bit lower.

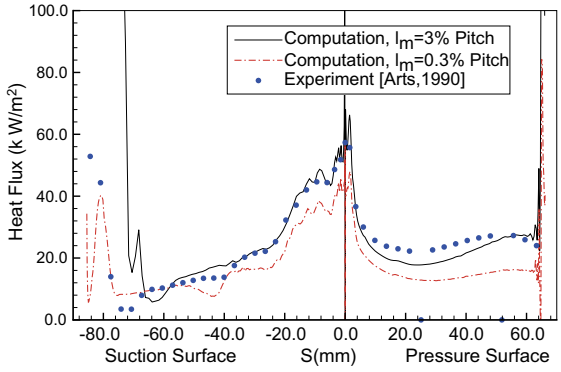

Fig. 6. Heat flux distributions for VKI MUR222.

5.3. VKI MUR222 test case: higher exit Mach number

In this case, the experimental isentropic Mach number is 1.1, the exit Reynolds number, 5×10^5, and the measured free stream turbulence level is 6%.

The predicted heat flux in Fig. 6, in contrast, presents a better agreement with the experimental data than that of the lower exit Mach number MUR235 case (shown in Fig. 5). Since in the high exit Mach number case, the acceleration is stronger and the boundary layer on the suction side remains laminar over a large part of the blade. The turbulence length scale l_m at 0.3% of pitch gives a most satisfactory result for the transition onset along the suction surface of the blade.

6. Conclusions

An efficient numerical method, MIFVS, has been extended to solve the transonic cascade flow and heat transfer in a highly loaded turbine blade. Key characteristics of the MIFVS solver include the establishment of an implicit formulation, eigenvalue analysis of the Jacobi matrices for the NS equations. Since matrix operations are not necessary in the implicit solver, computing efforts in each iteration step can be significantly reduced.

A low Reynolds number k–ϵ turbulence model, with the compressibility effect considered and the turbulence production term P_k modified near the blunt leading edge, and a transition model have been implemented into the MIFVS solver. Results obtained for the wave profiles, the surface isentropic Mach number distributions, Schlieren image and heat transfer show good agreements with the experimental data and other published calculation results. The important flow features are well predicted. By simulating this transonic transition flow, the extended MIFVS is demonstrated to be numerically efficient and accurate for the highly loaded turbine blade.

Acknowledgements

Professors Jung Y. Yoo (Seoul National University, Republic of Korea), Peter R. Voke (University of Surrey,

UK), Mark A.F. Kendall (University of Queensland, Australia) and Brian J. Bellhouse (University of Oxford, UK) are acknowledged for their insights and discussions.

References

Abu-Ghannam, B.J., Shaw, R., 1980. Natural transition of boundary layers—the effects of turbulence, pressure gradient, and flow history. Journal of Mechanical Engineering Science 22 (5), 213–228.

Arts, T., 1994. Highly loaded transonic and film cooed linear turbine guide vane cascadeVKI Lecture Series 1994-06. von Karman Institute for Fluid Dynamics, Belgium.

Arts, T., Lambert de Rouvroit, M., Rutherford, A.W., 1990. Aero-thermal investigation of a highly loaded transonic linear turbine guide vane cascade. VKI Technical Note 174, von Karman Institute for Fluid Dynamics, Belgium.

Chien, K.Y., 1982. Predictions of channel and boundary-layer flows with lower-Reynolds-number turbulence model. AIAA Journal 20 (1).

Chima, R.V., 1996. Application of the *k*–omega turbulence model to quasi-three-dimensional turbomachinery flows. Journal of Propulsion and Power 12 (6), 1176–1179.

Cho, N.-H., Liu, X., Rodi, W., Schonung, B., 1993. Calculation of wake-induced unsteady flow in a turbine cascade. ASME Journal of Turbomachinery 115, 675–686.

Craft, T.J., Launder, B.E., Suga, K., 1997. Prediction of turbulent transitional phenomena with a nonlinear eddy-viscosity model. International Journal of Heat and Fluid Flow 18 (1), 15–28.

Curtis, E.M., Hodson, H.P., Banieghbal, M.R., Denton, J.D., Howell, R.J., Harvey, N.W., 1996. Development of blade profiles for low pressure turbine applications. ASME Journal of Turbomachinery 119 (3), 531–538.

Gehrer, A., Jericha, H., 1998. External heat transfer predictions in a highly-loaded transonic linear turbine guide vane cascade using an upwind biased Navier–Stokes solver. ASME Paper 98-GT-238.

Granovskii, A.V., Karelin, A.M., Popov, K.M., 1995. Experimental investigation of flow structure and losses in a high load transonic turbine stage. AGARD-CP-571, UK.

Hall, U., Larsson, J., Bario, F., Kulisa, P., Slimani, J., Begin, V., Eriksson, L.-E., Wahlen, U., 1998. Simulations and measurements on impulse blades for heat transfer prediction in supersonic turbine applications. In: ASME 98-GT-154, Proceedings of the 1998 International Gas Turbine & Aeroengine Congress & Exhibition, Stockholm, Sweden.

Howell, R.J., Ramesh O.N., Hodson, H.P., Harvey N.W., Schulte, V., 2000. High loaded and aft loaded profiles for low pressure turbines. ASME Paper, 2000-GT-261.

Howell, R.J., Hodson, H.P., Schulte, V., Heinz-Peter Schiffer, Hasslebach, F., Harvey, N.W., 2001. Layer development in the BR710 and BR715 LP turbines – the implementation of high lift and ultra high lift concepts. In: Proceedings of the ASME Turbo EXPO 2001, New Orleans, LA, USA.

Kato, M., Launder, B.E., 1993. The modelling of turbulent flow around stationary and vibrating square cylinder. In: Proceedings of the 9th Symposium on Turbulent Shere Flows, Kyoto, Japan.

Liu, Y., Liu, B., Xiang, Y., 1996. A new highly efficient and accurate implicit flux vector splitting schemes. Chinese Science Bulletin 41 (14), 1229–1232.

Liu, Y., Bellhouse, B.J., 2005. Prediction of jet flows in the supersonic nozzle and diffuser. International Journal for Numerical Methods in Fluids 47, 1147–1155.

Liu, Y., Kendall, M.A.F., 2004. Numerical simulation of heat transfer from a transonic jet impinging on skin for needle-free powdered drug and vaccine delivery. Proceedings of the Institution of Mechanical Engineers, Part C: Journal of Mechanical Engineering Science 218 (11), 1373–1383.

Liu, Y., Zhang, Q., 2006. The implicit formulation of flux-vector-splitting scheme with application to transonic flows. International Journal of Mechanical Science 48 (11), 1208–1222.

Michelassi, V., Rodi, W., 1997. Experimental and numerical investigation of boundary-layer and wake development in a transonic turbine cascade. In: ASME 97-GT-483, Proceedings of the 1997 International Gas Turbine & Aeroengine Congress & Exposition, Orlando, FL, USA.

Sarkar, S., 2005. Wake-induced transitional flow over a highly-loaded LP turbine blade. In: ASME Turbo Expo 2005, ASME-GT-2005-68895, Reno-Tahoe, Nevada, USA.

Sarkar, S., Erlebacher, G., Hussaini, M.Y., Kreiss, H.O., 1991. The analysis and modelling of dilational terms in compressible turbulence. Journal of Fluid Mechanics 227, 473–493.

Segawa, K., Shikano, Y., Tsubouchi, K., 2001. Performance verification of a highly loaded steam turbine blade. JPGC2001/PWR-19125, New Orleans, LA, USA.

Steger, J.L., Warming, R.F., 1981. Flux vector splitting of the inviscid gas dynamic equations with application to finite-difference methods. Journal of Computational Physics 40.